



HAL
open science

Sub-Wavelength Arrays of Metallic Nanoparticles for Polarization-Selective Broad-Band Absorbers

Sophie Camelio, David Babonneau, Frédéric Pailloux, Sophie Rousselet, Elliot Vandenhecke

► **To cite this version:**

Sophie Camelio, David Babonneau, Frédéric Pailloux, Sophie Rousselet, Elliot Vandenhecke. Sub-Wavelength Arrays of Metallic Nanoparticles for Polarization-Selective Broad-Band Absorbers. *Nanoscience and Nanotechnology Letters*, 2013, 5 (1), pp.19-26. 10.1166/nnl.2013.1418. hal-04433115

HAL Id: hal-04433115

<https://hal.science/hal-04433115>

Submitted on 1 Feb 2024

HAL is a multi-disciplinary open access archive for the deposit and dissemination of scientific research documents, whether they are published or not. The documents may come from teaching and research institutions in France or abroad, or from public or private research centers.

L'archive ouverte pluridisciplinaire **HAL**, est destinée au dépôt et à la diffusion de documents scientifiques de niveau recherche, publiés ou non, émanant des établissements d'enseignement et de recherche français ou étrangers, des laboratoires publics ou privés.

Sub-wavelength arrays of metallic nanoparticles for polarization-selective broad-band absorbers

Sophie Camelio*, David Babonneau, Frédéric Pailloux, Sophie Rousselet, Elliot Vandennecke

Institut Pprime, Département Physique et Mécanique des Matériaux, UPR 3346 CNRS, Université de Poitiers, SP2MI, Téléport 2 – 11 Bvd. M. et P. Curie, BP 30179, 86962 Futuroscope Chasseneuil Cedex, France

Tel + 33 549 496 751 Fax +33 549 496 692 sophie.camelio@univ-poitiers.fr

Abstract

Sub-wavelength arrays of silver nanoparticles embedded in a dielectric matrix are elaborated by a low-cost bottom-up technique, which combines substrate pre-patterning by defocused ion-erosion (resulting in the generation of one-dimensional nanoripples) with subsequent Volmer-Weber growth by physical vapor deposition at glancing incidence. The arrays are constituted by regular chains (~20 nm period) of small particles (size less than 10 nm) with elongated shape in the direction of the ripples. This shape anisotropy and the resulting interparticle coupling inside the chains (gap between the particles less than 10 nm) are responsible for the plasmonic dichroism of the array leading to polarization-selective broad-band absorption in visible and near infrared. This dichroism can be tuned by adjusting the amount of deposited metal, the elaboration temperature, the nature of the dielectric host and the deposition geometry. The technique is at last employed to elaborate 3D nanostructures.

Introduction

With the aim of light trapping in thin-film silicon solar cells for achieving high efficiencies, new approaches based on metallic nanoparticles and metal nanostructures have been proposed. For example metallic nanoparticles placed on the top of c-Si solar cells have been shown to increase efficiency¹, several groups have reported enhanced absorption and photocurrent on a variety of solar cell designs by placing the nanoparticles near the absorber²⁻⁴. Indeed, the specific optical properties of metallic nanoparticles are a consequence of the appearance of a resonance in their absorption spectra; the so-called localized surface plasmon resonance (SPR) due to their strong interactions with light through the resonant excitations of the collective oscillations of the conduction electrons within the particles. The spectral position of the SPR, in the visible and near infrared, not only depends on the intrinsic properties of the metal and of the dielectric matrix surrounding the particles, but also on the morphology and spatial organization of the particles within the matrix. For sufficiently small particles (<50 nm), this absorption is accompanied by a strong enhancement of the electromagnetic field inside the particles and in the surrounding matrix making their utilization attractive if they are localized in the active layer of the solar cells.

A common way to control both the morphology and the spatial organization of the particles is to use electron-beam lithography and the standard liftoff process, which allows an accurate positioning of the particles on designed locations. However this top-down sample preparation is time consuming and leads to arrays of particles with sizes larger than 20 nm and gaps between the particles greater than 10 nm. Another method consists in using nanostructured surfaces as templates and a bottom-up approach to elaborate the particles. Faceted alumina substrates prepared by thermal treatment of vicinal surfaces can be used as efficient templates⁵⁻⁸, but their preparation requires very high temperatures (> 1000 °C) annealing

under oxygen atmosphere and is limited to crystalline materials. Another technical approach to produce nanostructured templates is to use surface erosion by ion sputtering at oblique incidence. This technique, which can be applied to a large variety of materials, from amorphous materials to crystalline semiconductors as well as metals and insulators, can produce regular and periodic surface structures in the form of ripples with well-defined lateral periodicity, vertical amplitude, and controlled orientation. The phenomenon is related to the interplay between ion erosion and the diffusion of adatoms, which induces surface reorganization⁹⁻¹². This low-cost and fast-output approach using surface erosion followed by physical vapor deposition of metal¹³⁻¹⁷ is very interesting for the production of thin film silicon solar cells, because it involves the same manufacturing technology namely thin-film coatings. Furthermore, the obtained nanoparticles exhibit a smaller edge-to-edge distances (less than 5 nm) than those obtained by lithography leading to a larger field amplification. In a previous paper¹⁵, we have shown that organized arrays of aligned silver nanoparticles can be obtained by grazing incidence ion-beam sputtering on nanopatterned alumina surface due to shadowing effects. In the present work, we show first that the preferential diffusion of silver atoms along the ripples, and therefore the spatial organization of the nanoparticles as linear chains, is limited after normal deposition. Moreover, the role of the temperature, of the amount of silver, of the nature of the rippled surface on the size, shape anisotropy and spatial organization of the particles is investigated in order to explain their optical properties. At last, we show that it is possible to increase the absorption intensity by elaborating ripple-based multilayers consisting of sequential deposition of silver on rippled thin-film of dielectric material.

Sample preparation and characterization

Several $\text{Al}_2\text{O}_3/\text{Ag}/\text{Al}_2\text{O}_3$ trilayers consisting of Ag nanoparticles sandwiched between amorphous Al_2O_3 films have been synthesized by alternate ion beam sputtering in a Nordiko3000 vacuum chamber. The sample preparation has been depicted in details elsewhere¹⁵ and consists in combining substrate pre-patterning by defocused ion-erosion with subsequent Volmer-Weber growth by physical vapor deposition. Firstly, rippled surfaces were produced on amorphous Al_2O_3 thin films (~ 70 nm in thickness before erosion) deposited by ion-beam sputtering onto commercially available fused silica for optical measurements and carbon coated grids for high-angle annular dark-field scanning transmission electron microscopy (HAADF-STEM) characterizations. Ion-erosion was performed at room temperature with Xe^+ ions at a sputtering angle of $\theta = 55^\circ$ with respect to the surface normal, with an ion energy $E = 1000$ eV, and a fluence of about 3.6×10^{16} ions. cm^{-2} (ion flux $\sim 2 \times 10^{14}$ ions $\text{cm}^{-2} \cdot \text{s}^{-1}$, at an erosion rate of 0.28 nm. s^{-1}). For this purpose, the sputtering chamber includes a plasma bridge constituted by a filament-less RF-ion gun (with a multicusp and two molybdenum grids) followed by a filament-less neutralizer (hollow cathode) in order to avoid space charge during the ion transport and also at the sample holder, connected to ground. The pattern obtained from ion-erosion consists in periodic ripples that are oriented perpendicular to the ion beam and with a period in the range from 20 nm to 25 nm. Secondly, the rippled thin films were used as templates in order to create self-organized chains of silver nanoparticles. Deposition of Ag was accomplished by ion-beam sputtering essentially at room temperature and at a glancing incidence of 5° from the surface, perpendicularly to the ripples in order to produce aligned nanoparticles since deposition parallel to ripples does not¹⁸. Nevertheless samples obtained at 200°C or at normal incidence have also been investigated. The effective Ag thickness t_{Ag} was varied between 0.7 nm and 2.8 nm. Then, an Al_2O_3

capping-layer (~ 15 nm in thickness) was deposited on the nanoparticles. For comparison, an $\text{Al}_2\text{O}_3/\text{Ag}/\text{Al}_2\text{O}_3$ trilayer obtained on an unstructured flat surface with Ag deposition at normal incidence was also prepared, as well as $\text{Si}_3\text{N}_4/\text{Ag}/\text{Si}_3\text{N}_4$ and $\text{BN}/\text{Ag}/\text{BN}$ trilayers. $\text{Al}_2\text{O}_3/\text{Ag}/\text{Al}_2\text{O}_3/\text{Ag}/\text{Al}_2\text{O}_3$ multilayers were also elaborated for which both the first and second Al_2O_3 buffer layers were pre-patterned by ion erosion. All the samples are listed in Table 1.

The morphology of the patterned surfaces films was characterized by Atomic Force Microscopy (AFM) in the tapping mode, followed by a quantitative study of the Power Spectral Density (PSD) of the images which performs a decomposition of the surface profile into its spatial wavelengths and thus provides useful information on characteristic features which compose the topography of the films. The morphology and the spatial organization of the nanoparticles were characterized from in-plane views by HAADF-STEM with a JEOL 2200FS microscope using an acceleration voltage of 200 kV (Schottky-FEG), a probe size of 0.7 nm, and an inner collection angle of 50 mrad. The optical properties were investigated by means of spectroscopic transmission of polarized light at normal incidence in the range between 250 nm and 1200 nm by using a Cary5000 spectrophotometer from Agilent Technologies equipped with a rotating polarizer.

Results and discussion

When the growth of silver is performed at normal incidence on flat Al_2O_3 surface (Sample A with $t_{\text{Ag}} = 1.8$ nm) the metallic nanoparticles are randomly distributed on the surface and their average in-plane shape is isotropic (Figure 1a). The areal density δ , surface coverage τ and the mean in-plane particle size $\langle D \rangle$ (and corresponding standard deviation σ), which depend on

the effective thickness of silver, can be retrieved (Table 2) from a quantitative analysis of the HAADF-STEM plane-view image. The mean center-to-center distance between the nanoparticles $L = 11.8$ nm is obtained from the autocorrelation function of the image (Figure 1b) showing a circular ring typical of an isotropic spatial organization. As we have already shown in previous papers¹⁹⁻²¹, the particles obtained in such elaboration conditions are spheroidal in average with an out-of-plane aspect ratio H/D (with H , the height of the nanoparticles) smaller than one, which decreases when D increases. Therefore, Sample A presents a unique SPR at $\lambda = 518$ nm (Figure 1e) that can be adjusted by varying the effective thickness of silver, i.e. the mean $\langle H/D \rangle$ value.

Figure 1c shows the in-plane organization and the morphology of Ag nanoparticles deposited at normal incidence on a rippled Al_2O_3 surface (Sample B) for the same equivalent thickness of silver ($t_{\text{Ag}}=1.8$ nm). At first glance of the HAADF-STEM image, one may say that the presence of ripples on the surface leads to a tendency towards a spatial organization of the particles. Moreover, the autocorrelation image (Figure 1d) still presents an almost circular ring at the center but also exhibits horizontal lines with a period of 18.8 nm, contrary to the previous case. However, a quantitative analysis shows that sample B is not so different from sample A. Indeed, the areal density δ and surface coverage τ are similar, as well as the mean in-plane size $\langle D \rangle$. This shows that the nucleation of the particles is mainly affected by the density of point defects on the surface (atomic scale surface corrugation) and very little by the presence of ripples (nanometric scale surface corrugation). The mean in-plane projected sizes $\langle D_{//} \rangle$ and $\langle D_{\perp} \rangle$ along the directions parallel and perpendicular to the ripples ($\langle D \rangle = (\langle D_{//} \rangle \cdot \langle D_{\perp} \rangle)^{1/2}$), together with the corresponding standard deviations $\sigma_{//}$ and σ_{\perp} are reported in Table 2, as well as the mean center-to-center distance between the particles along the directions parallel ($L_{//}$) and perpendicular (L_{\perp}) to the ripples. The particles are slightly

elongated along the ripples direction ($\frac{\langle D_{//} \rangle}{\langle D_{\perp} \rangle} = 1.05$) with a weak anisotropic in-plane

organization ($\frac{\langle L_{//} \rangle}{\langle L_{\perp} \rangle} = 0.98$), that shows a slight preferential diffusion of silver atoms along the

ripples. We can notice in Figure 1e, that the optical transmittance of such a nanoparticle

assembly depends on the direction of the electromagnetic field compared to the direction of

the ripples since the resonance is divided into two contributions: the one obtained when the

polarization is longitudinal ($\lambda_{//} = 522$ nm) along the ripples direction and the other obtained

with a polarization transverse ($\lambda_{\perp} = 506$ nm) to the ripples direction. The plasmonic splitting,

$\Delta\lambda = \lambda_{//} - \lambda_{\perp}$, between the position of the two SPRs is positive in agreement with $\frac{\langle D_{//} \rangle}{\langle D_{\perp} \rangle} > 1$

and $\frac{\langle L_{//} \rangle}{\langle L_{\perp} \rangle} < 1$ (see ref. 22 and 23). However $\Delta\lambda$ is very weak (16 nm) and therefore silver

deposition at normal incidence on a rippled surface does not lead to a spectacular change of

the optical properties. Let us note that when the Ag growth is performed at a higher

temperature (at normal incidence on a rippled Al_2O_3 surface, sample not shown), the pattern

also lacks of optical anisotropy (for example, $\Delta\lambda = \lambda_{//} - \lambda_{\perp} = 20$ nm for $t_{\text{Ag}}=2.5$ nm at 300°C).

In order to take advantage of shadowing effects, silver has to be deposited on the

nanostructured surface at a glancing angle (5° from the surface) perpendicularly to the ripples

direction. This has been done for sample C with an effective thickness t_{Ag} of 1.4 nm. The

HAADF-STEM image presented in Figure 2a shows ellipsoidal Ag nanoparticles organized

along linear chains with a period corresponding to that of the ripples ($L_{\perp} = 21.5$ nm)

suggesting that the periodicity is imposed by the pre-patterned Al_2O_3 surface¹³⁻¹⁷. In these

conditions of elaboration (i.e. at glancing incidence), while the nanoparticles present a mean

in-plane size $\langle D \rangle = 4.5$ nm smaller than the one obtained at normal incidence with $t_{\text{Ag}} = 1.8$

nm (Samples A and B), the in-plane distribution of the particles becomes more anisotropic ($\frac{\langle L_{//} \rangle}{\langle L_{\perp} \rangle} = 0.51$) as well as their in-plane shape (with $\frac{\langle D_{//} \rangle}{\langle D_{\perp} \rangle} = 1.09$). As seen in Figure 3a, the structural anisotropy of such planar arrays of Ag nanoparticles results in a dependence of their optical transmittance on the polarization of the incident light, with two SPRs located at $\lambda_{//} = 495$ nm and $\lambda_{\perp} = 465$ nm (Table 1). The shift of these positions as well as the decrease in the amplitude of the resonances compared to those obtained with Samples A and B may be ascribed to the smaller size of the particles and therefore to smaller out-of-plane aspect ratio H/D and volume. Whereas the splitting ($\Delta\lambda = 30$ nm) of the SPRs is commonly attributed in the literature to the anisotropic spatial organization of the particles with a preferential electromagnetic coupling of the particles inside the chains ($L_{//} - \langle D_{//} \rangle = 6.2$ nm), it may be also attributed to the increase of the $\frac{\langle D_{//} \rangle}{\langle D_{\perp} \rangle}$ value. In Figure 2a, we can notice the presence of very small particles between the chains with diameter less than 4 nm, which suggests firstly that the nucleation of silver takes place on the whole surface at the beginning of the deposition and secondly that the particle growth is favored on the facets of the ripples exposed to the Ag flux by shadowing effects. This is confirmed in Figure 2b that shows the HAADF-STEM image of Sample E where the effective thickness t_{Ag} is reduced to 0.7 nm. This low Ag coverage leads to an almost isotropic organization of small spheroidal nanoparticles ($L_{//} \sim L_{\perp} \sim 7.7$ nm and $\langle D_{//} \rangle \sim \langle D_{\perp} \rangle \sim 3.2$ nm), despite shadowing effects, and therefore to almost isotropic optical properties (Figure 3b). Again, these results confirm that the nucleation is not influenced by the presence of ripples (even at grazing incidence) probably because the amorphous surface remains “atomically flat” and that the diffusion length of silver atoms is much larger than the ripples period, i.e. the nucleation is not limited to the areas illuminated by the silver atomic flux, in contrast to the growth. A deposition of silver at a temperature of

200°C was performed with the same effective thickness of 1.4 nm (Sample D) on a pre-patterned Al₂O₃ thin film. As expected, compared to Sample C, the areal density δ decreases, the particles are bigger ($\langle D \rangle = 8.0$ nm), they are still organized in linear periodic chains (Figure 2c) but their spatial organization is less anisotropic ($\frac{\langle L_{//} \rangle}{\langle L_{\perp} \rangle} = 0.71$, with $L_{//} - \langle D_{//} \rangle = 7.8$ nm) showing that the temperature reduces the preferential diffusion of silver atoms along the ripples and therefore the plasmonic dichroism of the sample is reduced ($\Delta\lambda=20$ nm).

Actually, higher plasmonic dichroism $\Delta\lambda$ can be achieved at room temperature by increasing the effective thickness of silver in order to promote the lateral growth of the particles in the direction parallel to the ripples. Indeed, for $t_{Ag} = 2.8$ nm (Sample F), agglomeration and coarsening lead to the formation of elongated nanoparticles predominantly aligned along the direction of the ripples (i.e., perpendicular to the silver atomic flux) with $\frac{\langle D_{//} \rangle}{\langle D_{\perp} \rangle} = 1.40$ and

$\frac{\langle L_{//} \rangle}{\langle L_{\perp} \rangle} = 0.70$ (Figure 2d and Table 2). Therefore, for a transverse excitation, the transmittance

T_{\perp} shows a localized SPR whose spectral position changes from 457 nm (Sample E) to 465 nm (Sample C) and 487 nm (Sample F) when t_{Ag} increases from 0.7 nm to 1.4 nm and 2.8 nm respectively (Table 1). This spectral shift can be ascribed to a decrease of the out-of-plane ratio of the particles. In addition, the progressive increase of the amplitude of the resonance (Figures 3a and 3b) is due to the increase of the nanoparticle volume and of the surface coverage τ . In the case of high coverage ($t_{Ag} = 2.8$ nm - Sample F) with nanoparticles still disconnected (Figure 2d), the longitudinal transmittance $T_{//}$ displays a very broad-band absorption which tends to a spectral behavior characteristic of infinite metal nanowires. The anisotropic shape and anisotropic spatial organization are both responsible to this behavior. It has to be noticed here that the mean edge-to-edge distance between the nanoparticles is less

than 10 nm ($L_{//} - \langle D_{//} \rangle = 5.4$ nm), a distance that cannot be reached with lithographic methods so far, due to proximity effects. Accordingly, it is possible to design plasmonic nanostructures capable of an efficient absorption of light in the visible and in the near infrared depending on the polarization of the incident light, with a strong local field enhancement in the interparticle gap.

The method presented so far offers many advantages since it is applicable to a wide range of materials. As an example, we show in figures 4a-c, for comparison, the surface topographies obtained by AFM of different dielectric materials (respectively Al_2O_3 , Si_3N_4 , BN) after ion-erosion performed with the same experimental conditions. At a first glance, we can see that the pattern characteristics are more or less similar for Al_2O_3 and Si_3N_4 materials while the rippled BN film exhibits a less ordered surface. This is quantitatively confirmed with the 1D Power Spectral Density of the images presented in figure 4d. From these curves, the period of the ripples can be retrieved from the position of the main peak: 20.7 nm, 24.7 nm and 19.5 nm for Al_2O_3 , Si_3N_4 and BN respectively. We can notice that the width w of the peak, that gives evidence of the ordering of the pattern, is narrower for Al_2O_3 film ($w = 0.0137 \text{ nm}^{-1}$) than for Si_3N_4 film ($w = 0.0176 \text{ nm}^{-1}$) and for BN film ($w = 0.0294 \text{ nm}^{-1}$) confirming that, with these energy, fluence and ion flux, and angle of erosion, the pattern obtained on the Al_2O_3 film is much more organized.

Figures 5a-b display the HAADF-STEM images obtained after deposition at grazing incidence of silver on pre-patterned Si_3N_4 (Sample G) and BN (Sample H) surfaces. Although the capping layer depositions were done at 200°C in order to obtain the right stoichiometry for the matrix, the effective thickness of silver is $t_{\text{Ag}} = 2.8$ nm as in the case of Sample F with an Al_2O_3 matrix deposited at room temperature. We can notice that the particles of samples G and H are organized in form of linear chains and exempt from very

small particles, probably due to the temperature during the elaboration process. The 1D PSD obtained from the binarized HAADF-STEM images of Samples F, G and H, are given in figure 5c. In the transverse direction, the 1D PSD exhibits a narrow first peak, from which it is possible to retrieve the mean distance between the particles chain, which is smaller for a BN matrix ($L_{\perp} = 16.5$ nm) than for a Si_3N_4 matrix ($L_{\perp} = 21$ nm), or an Al_2O_3 matrix ($L_{\perp} = 20.8$ nm). This result confirms that the lateral periodicity of the chains replicates the period of the ripples induced by ion erosion at glancing incidence, which depends itself on the nature of the material. Again, we can notice that the width w of the peak is narrower for Al_2O_3 film ($w = 0.007$ nm⁻¹) than for Si_3N_4 film ($w = 0.009$ nm⁻¹) and for BN film ($w = 0.012$ nm⁻¹). In the longitudinal direction, the 1D PSD presents a single peak broader than the previous one indicating that the particles are less ordered in this direction (i.e. inside the chains). Moreover,

the nanoparticles are less elongated, $\frac{\langle D_{\parallel} \rangle}{\langle D_{\perp} \rangle} = 1.14$ for Sample G and $\frac{\langle D_{\parallel} \rangle}{\langle D_{\perp} \rangle} = 1.11$ for Sample

H, compared to Sample F ($\frac{\langle D_{\parallel} \rangle}{\langle D_{\perp} \rangle} = 1.40$). This result can be attributed to the elaboration

temperature of Samples G and H (200°C) but the small shape anisotropy of Sample H may also originate from the patterned BN surface which exhibits a lower quality, decreasing therefore the preferential diffusion along the ripples of the silver atoms. The transmittance spectra presented in Figure 5d confirm first that the spectral positions and widths of the SPRs depend on the dielectric function of the surrounding material, $\epsilon_{\text{BN}} \sim \epsilon_{\text{Al}_2\text{O}_3} < \epsilon_{\text{Si}_3\text{N}_4}$ leading to a spectral position of the SPRs blue-shifted for Sample H compared to Sample G. Secondly, the splitting of the SPRs, $\Delta\lambda$, is also matrix-dependent ($0 < \Delta\lambda_{\text{BN}} < \Delta\lambda_{\text{Si}_3\text{N}_4}$) which is in

agreement with $1 < \frac{\langle D_{\parallel} \rangle}{\langle D_{\perp} \rangle}_{\text{BN}} < \frac{\langle D_{\parallel} \rangle}{\langle D_{\perp} \rangle}_{\text{Si}_3\text{N}_4}$. On the other hand, the spatial organization $\frac{\langle L_{\parallel} \rangle}{\langle L_{\perp} \rangle} =$

1 for Sample G (Si_3N_4 matrix) is not supposed to lead to a plasmonic splitting, whereas

$\frac{\langle L_{//} \rangle}{\langle L_{\perp} \rangle} = 1.3$ for Sample H (BN matrix) should lead to a negative splitting (the particles are closer in the transverse direction than in the longitudinal one). However the plasmonic splitting $\Delta\lambda$ is still positive in both cases, suggesting that it is mainly due to the anisotropic shape of the nanoparticles and not to the spatial anisotropy.

At last, multilayer samples consisting of 3D arrays of nanoparticle chains can also be produced at fast output and low production costs with this bottom-up approach²⁴. As an example we have fabricated, at room temperature, Al₂O₃/Ag/Al₂O₃/Ag/Al₂O₃ multilayers with this technique, by depositing first an Al₂O₃/Ag/Al₂O₃ in a similar way as previously (with $t_{\text{Ag}} = 1.5$ nm) but the second Al₂O₃ layer was thick enough to perform a second ion erosion by Xe ions (with a final thickness estimated to 20 nm after the patterning). Then a second deposition of silver (with $t_{\text{Ag}} = 1.5$ nm) was performed followed by the deposition of an Al₂O₃ capping-layer (with a thickness of 20 nm). Two configurations were tested: a parallel configuration where the directions of the particle chains in both layers are parallel (Sample I), and a transverse configuration where the directions of the chains are perpendicular (Sample J), i.e. the sample was tilted by 90° at the end of the deposition of the thick intermediate Al₂O₃ layer and before ion erosion. The vertical spacing of the two nanoparticle layers is high enough to neglect a vertical electromagnetic coupling between the particles. The optical properties of Sample I and J are plotted in Figure 5, which exhibits also the optical properties of a corresponding single Al₂O₃/Ag/Al₂O₃ trilayer. We can notice that both the multilayer in parallel configuration (Sample I) and this single trilayer display two SPRs located at 492 nm and 545 nm for transverse and longitudinal excitation respectively. This result shows therefore that it is possible to maintain the plasmonic dichroism within this 3D configuration, while the amplitude of the absorption is increased. On the contrary, in the transverse configuration (Sample J) the absorption bands are no more polarization-selective since the

spectral position of the SPR is identical for transverse and longitudinal excitation, i.e. even if the particles are organized in linear chains within each layer, the whole 3D arrangement behaves as an isotropic medium.

Conclusion

Sub-wavelength arrays of small silver nanoparticles (with size smaller than 10 nm, transverse period around 20-25 nm and longitudinal interparticle gap less than 10 nm) have been elaborated by combining substrate pre-patterning by defocused ion-erosion with subsequent Volmer-Weber growth by physical vapor deposition at glancing incidence. In this article, we have shown that the nucleation of the particles on the nanostructured (rippled) surface is isotropic while their growth is favored along the longitudinal direction (parallel to the ripples) by shadowing effects. Therefore the nanoparticle shape anisotropy depends on the effective thickness of the deposited metal. Also the temperature during the metal deposition and the nature of the rippled surface play a significant role on the resulting elongated shape and spatial organization. This shape anisotropy and the resulting interparticle coupling inside the chains are responsible for the plasmonic dichroism of the array leading to polarization-selective broad-band absorption. This low cost technique can also be employed to fabricate 3D nanostructures by superimposing the sub-wavelength arrays of particles. We have demonstrated that it is possible to increase the absorption while keeping the original dichroism through the stack (providing the direction of the particles chains in each layer remains parallel). At last, since the pattern characteristics (period and ordering of the ripples) depend on the nature of the sputtered material but also on the ion energy, the angle of incidence, the fluence, the temperature^{25,26} it would be interesting in the future to deepen the role of these parameters on the organization and shape of the nanoparticles and therefore on

the optical dichroism.

Acknowledgements

The authors want to thank Philippe Guérin for assistance during the elaboration of the samples.

References

- 1- S. Pillai and M. A. Green, *Sol. Energy Mater. Sol. Cells*, 94, 1481–6 (**2010**)
- 2- D. Derkacs, S. H. Lim, P. Matheu, W. Mar and E. T. Yu, *Appl. Phys. Lett.*, 89, 093103 (**2006**)
- 3- F.-C. Chen, J.-L. Wu, C.-L. Lee, Y. Hong, C.-H. Kuo and M. H. Huang, *Appl. Phys. Lett.*, 95, 013305 (**2009**)
- 4- D. Duché, P. Torchio, L. Escoubas, F. Monestier, J.-J. Simon, F. Flory, G. Mathian, *Sol. Energy Mater. Sol. Cells*, 93, 1377-1382 (**2009**)
- 5- A. Sugawara, T. Coyle, G. G. Hembree and M. R. Scheinfein, *Appl. Phys. Lett.*, 70, 1043 (**1997**)
- 6- S. Camelio, D. Babonneau, D. Lantiat and L. Simonot, *EPL*, 79, 47002 (**2007**)
- 7- R. Verre, K. Fleischer, J.F. McGilp, D. Fox, G. Behan, H. Zhang, I.V. Shvets, *Nanotechnology*, 23, 035606 (**2012**)
- 8- R.Verre, K. Fleischer, O. Ualibek, and I. V. Shvets, *Appl. Phys. Lett.*, 100, 031102 (**2012**)
- 9- T. M. Mayer, E. Chason, and A. J. Howard, *J. Appl. Phys.*, 76,1633 (**1994**)
- 10- C. C. Umbach, R. L. Headrick, and K.-C. Chang, *Phys. Rev.Lett.*, 87, 246104 (**2001**)
- 11- G. Carter and V. Vishnyakov, *Phys. Rev. B*, 54, 17647 (**1996**)
- 12- A. Keller, S. Facsko, *Materials*, 3, 4811-4841 (**2010**)

- 13- T. W. H. Oates, A. Keller, S. Facsko and Mücklich A., *Plasmonics*, 2, 47 (2007)
- 14- A. Toma, D. Chiappe, D. Massabo, C. Boragno and de Mongeot F. B., *Appl. Phys. Lett.*, 93, 163104 (2008)
- 15- S. Camelio, D. Babonneau, D. Lantiat, L. Simonot and F. Pailloux, *Phys. Rev. B*, 80, 155434 (2009)
- 16- M. Ranjan, T. W. H. Oates, S. Facsko and W. Möller, *Opt. Lett.*, 35, 2576 (2010)
- 17- D. Babonneau, S. Camelio, L. Simonot, F. Pailloux, P. Guérin, B. Lamongie and O. Lyon, *EPL*, 93, 26005 (2011)
- 18- S. A. Khan, D. K. Avasthi, D. C. Agarwal, U. B. Singh and D. Kabiraj, *Nanotechnology*, 22, 235305 (2011)
- 19- J. Toudert, S. Camelio, D. Babonneau, M.-F. Denanot, T. Girardeau, J. P. Espinos, F. Yubero, and A. R. Gonzalez-Elipé, *J. Appl. Phys.* 98, 114316 (2005)
- 20- D. Lantiat, D. Babonneau, S. Camelio, F. Pailloux, and M.-F. Denanot, *J. Appl. Phys.* 102, 113518 (2007)
- 21- D. Babonneau, D. Lantiat, S. Camelio, L. Simonot, F. Pailloux, M.-F. Denanot, and T. Girardeau, *Eur. Phys. J.: Appl. Phys.* 44, 3–9 (2008)
- 22- W. Rechberger, A. Hohenau, A. Leitner, J.R. Krenn, B. Lamprecht, F.R. Aussenegg *Optics Communications* 220, 137 (2003)
- 23- C. Noguez, *J. Phys. Chem. C*, 111, 3806 (2007)
- 24- M. Buljan, J. Grenzer, A. Keller, N. Radić, V. Valeš, S. Bernstorff, T. Cornelius, H. T Metzger and V. Holý, *Phys. Rev B* 82, 125316 (2010)
- 25- U. Valbusa, C. Boragno, and F. Buatier de Mongeot, *J. Phys. Condens. Matter* 14, 8153 (2002)
- 26- W. L. Chan and E. Chason, *J. Appl. Phys.* 101, 121301 (2007)

Sample name	Incidence angle for Ag deposition (°)	Type of surface	Dielectric host	Temperature (°C)	Effective thickness of silver t_{Ag} (nm)	$\lambda_{//}$ (nm)	λ_{\perp} (nm)
A	Normal 90°	flat	Al ₂ O ₃	20	1.8	518	
B	Normal 90°	rippled	Al ₂ O ₃	20	1.8	522	506
C	Grazing 5°	rippled	Al ₂ O ₃	20	1.4	495	465
D	Grazing 5°	rippled	Al ₂ O ₃	200	1.4	482	462
E	Grazing 5°	rippled	Al ₂ O ₃	20	0.7	452	457
F	Grazing 5°	rippled	Al ₂ O ₃	20	2.8	613	487
G	Grazing 5°	rippled	Si ₃ N ₄	200	2.8	666	595
H	Grazing 5°	rippled	BN	200	2.8	541	497
I	Grazing 5°	rippled (twice)	Al ₂ O ₃	20	1.5 (twice)	545	492
J	Grazing 5°	rippled (twice)	Al ₂ O ₃	20	1.5 (twice)	496	494

Table 1 : List of the different samples elaborated by ion sputtering of silver on unstructured (Sample A) and nanostructured (Samples B-J) surfaces : Al₂O₃/Ag/Al₂O₃ trilayers (Samples A-F), Si₃N₄/Ag/Si₃N₄ trilayer (Sample G), BN/Ag/BN trilayer (Sample H) and Al₂O₃/Ag/Al₂O₃/Ag/Al₂O₃ multilayers (Samples I and J). Spectral position of the SPRs for transverse λ_{\perp} and longitudinal excitation $\lambda_{//}$ respectively.

Sample	δ (part/ μm^2)	τ (%)	$L_{//}$ (nm)	L_{\perp} (nm)	$\langle D \rangle$ (nm)	σ (nm)	$\langle D_{//} \rangle$ (nm)	$\sigma_{//}$ (nm)	$\langle D_{\perp} \rangle$ (nm)	σ_{\perp} (nm)
A	8540	35.5	11.8		7.0	1.81	-			
B	8770	32.5	11.8	12.0	6.7	1.85	6.9	2.05	6.6	1.89
C	13443	27	11.0	21.5	4.6	1.21	4.8	1.30	4.4	1.26
D	4576	28.8	16.2	22.7	8.0	3.28	8.4	3.17	7.7	3.47
E	15100	13.6	7.7	7.75	3.3	0.85	3.2	0.80	3.4	0.88
F	4172	22.3	14.5	20.8	7.7	3.18	9.1	3.57	6.5	2.99
G	4380	40.5	21	21	10.2	3.94	10.9	4.17	9.6	3.88
H	3580	35	21.5	16.5	10.5	2.5	11.1	3.4	10	1.83

Table 2 : Structural parameters retrieved from the quantitative analysis of the HAADF-STEM images : areal density δ and surface coverage τ , in-plane mean projected sizes $\langle D_{//} \rangle$ and $\langle D_{\perp} \rangle$ and corresponding standard deviations $\sigma_{//}$ and σ_{\perp} , mean interparticle distance along the ripples $L_{//}$ and perpendicular to the ripples L_{\perp} .

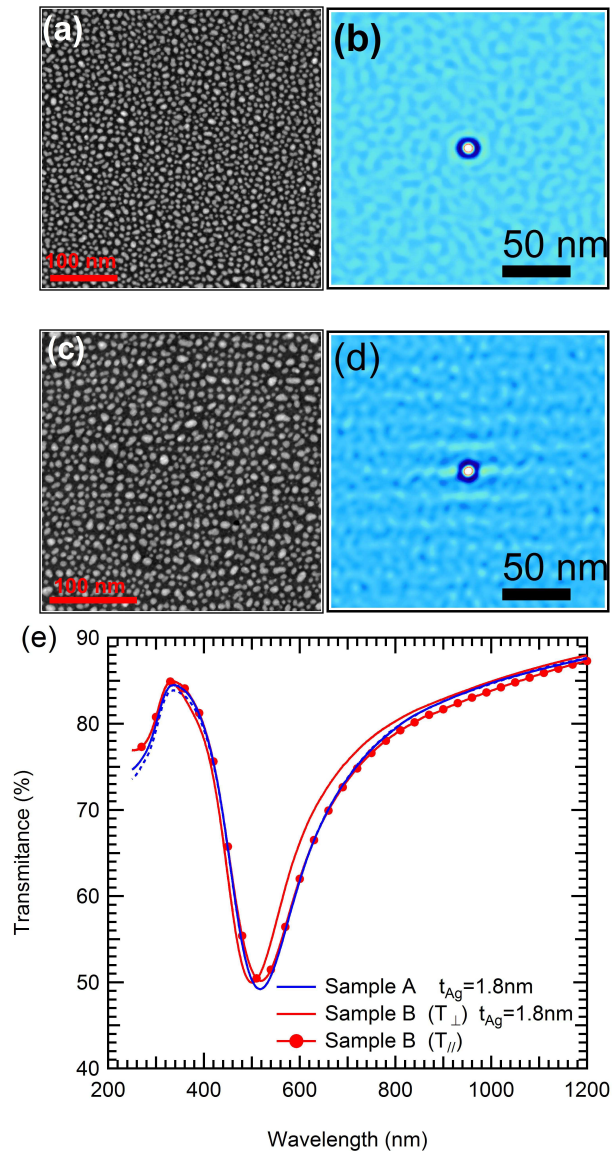


Figure 1 : Plane-view HAADF-STEM images of $\text{Al}_2\text{O}_3/\text{Ag}/\text{Al}_2\text{O}_3$ trilayers after normal silver deposition. The effective thickness is $t_{\text{Ag}} = 1.8$ nm. Silver deposition was made (a) on flat surface (Sample A) and (c) on rippled surface (Sample B). Autocorrelation function of the images of (b) Sample A and (d) Sample B. (e) Corresponding transmission measurements at normal incidence with the polarization of the incoming light being oriented parallel (T_{\parallel}) and perpendicular (T_{\perp}) to the ripples.

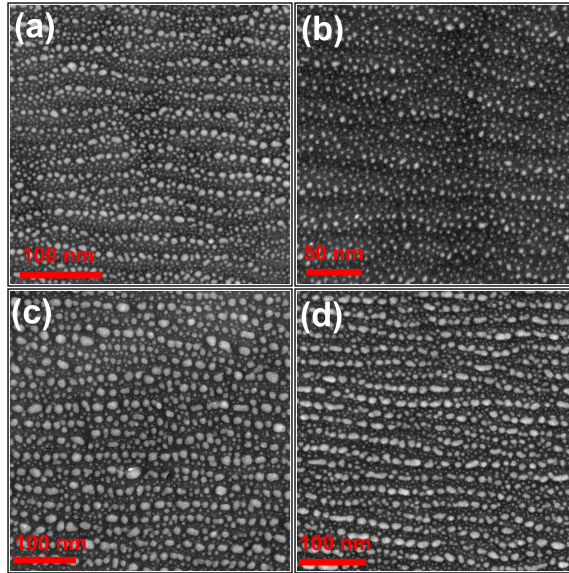


Figure 2 : Plane-view HAADF-STEM images of rippled $\text{Al}_2\text{O}_3/\text{Ag}/\text{Al}_2\text{O}_3$ trilayers after glancing-angle (5°) Ag deposition. The effective thicknesses are (a) $t_{\text{Ag}} = 1.4$ nm at room temperature (Sample C), (b) $t_{\text{Ag}} = 0.7$ nm at room temperature (Sample E), (c) $t_{\text{Ag}} = 1.4$ nm at 200°C (Sample D) and (d) $t_{\text{Ag}} = 2.8$ nm at room temperature (Sample F).

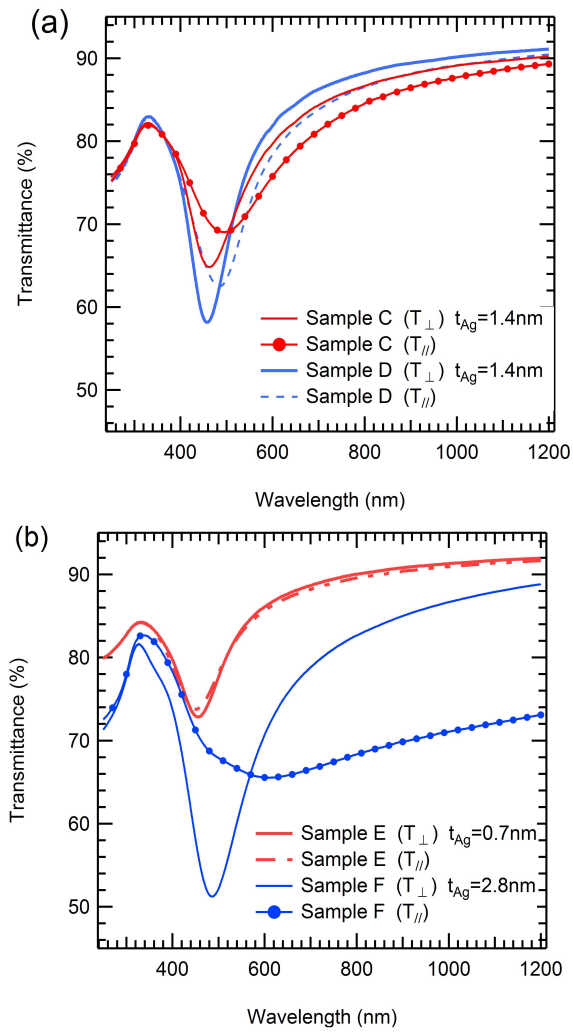


Figure 3 : Transmission measurements at normal incidence with the polarization of the incoming light being oriented parallel (T_{\parallel}) and perpendicular (T_{\perp}) to the ripples obtained on (a) Samples C and D (b) Samples E and F.

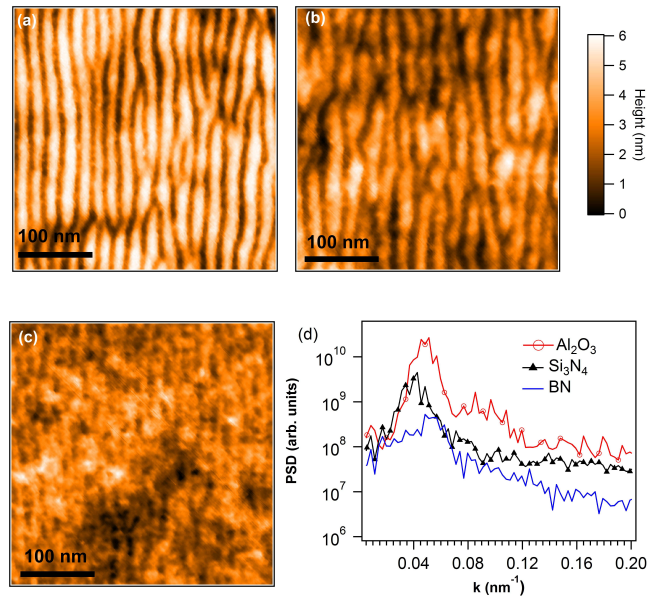


Figure 4 : AFM topographic image of different dielectric thin film etched during 180 s with 1keV-Xe+ ions at 55° with respect to the surface normal. (a) Al₂O₃, (b) Si₃N₄, (c) BN.

(d) Corresponding 1D Power Spectral Density (PSD) as a function of wave vector k.

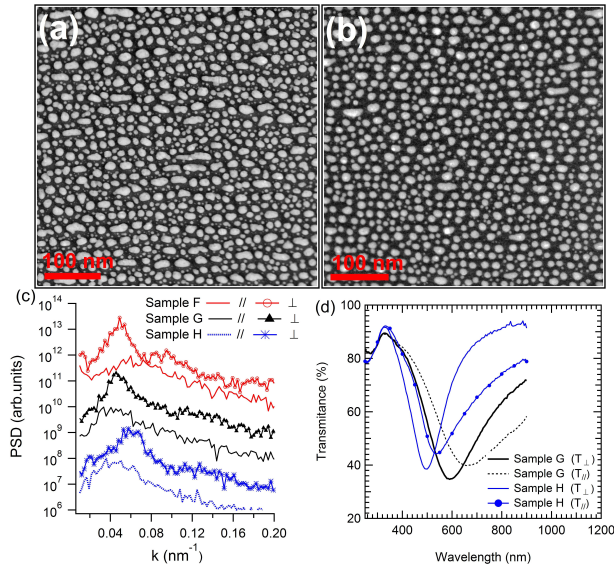


Figure 5 : Plane-view HAADF-STEM images of (a) rippled $\text{Si}_3\text{N}_4/\text{Ag}/\text{Si}_3\text{N}_4$ trilayer (Sample G) and (b) rippled $\text{BN}/\text{Ag}/\text{BN}$ trilayer (Sample H), after glancing-angle (5°) Ag deposition. The effective thicknesses are $t_{\text{Ag}} = 2.8$ nm, depositions were made at 200°C .

(c) Linear profiles of the PSD of the HAADFSTEM images of figures 2d (Sample F), 5a (Sample G) and 5b (Sample H), along two directions of the surface (parallel and transverse to the particles chains). For sake of clarity, the curves have been vertically translated.

(d) Transmission measurements at normal incidence on Samples H and G with the polarization of the incoming light being oriented parallel ($T_{//}$) and perpendicular (T_{\perp}) to the ripples.

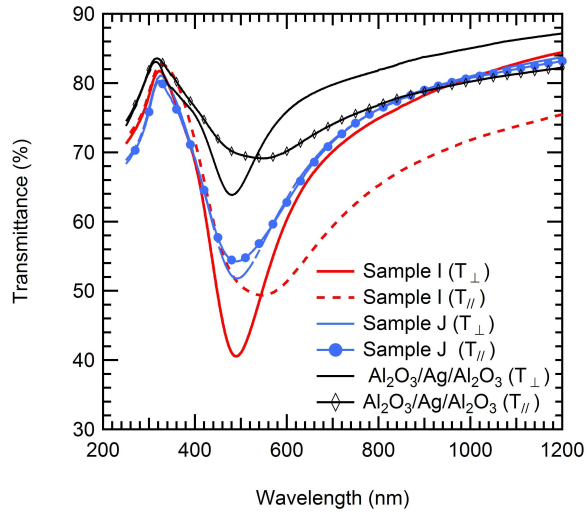


Figure 6 : Transmission measurements at normal incidence with the polarization of the incoming light being oriented parallel ($T_{//}$) and perpendicular (T_{\perp}) to the ripples obtained on the $\text{Al}_2\text{O}_3/\text{Ag}/\text{Al}_2\text{O}_3/\text{Ag}/\text{Al}_2\text{O}_3$ multilayers with a parallel configuration (Samples I) and transverse configuration (Sample J). The black curves represent the transmission measurements obtained on the $\text{Al}_2\text{O}_3/\text{Ag}/\text{Al}_2\text{O}_3$ intermediate trilayer.